Molecular Therapy
Nucleic Acids
Original Article

Improved Double-Nicking Strategies for *COL7A1*-Editing by Homologous Recombination

Thomas Kocher,[1,3] Roland N. Wagner,[1,3] Alfred Klausegger,[1] Christina Guttmann-Gruber,[1] Stefan Hainzl,[1] Johann W. Bauer,[2] Julia Reichelt,[1] and Ulrich Koller[1]

[1]EB House Austria, Research Program for Molecular Therapy of Genodermatoses, Department of Dermatology and Allergology, University Hospital of the Paracelsus Medical University Salzburg, 5020 Salzburg, Austria; [2]Department of Dermatology and Allergology, University Hospital of the Paracelsus Medical University Salzburg, 5020 Salzburg, Austria

Current gene-editing approaches for treatment of recessive dystrophic epidermolysis bullosa (RDEB), an inherited, severe form of blistering skin disease, suffer from low efficiencies and safety concerns that complicate implementation in clinical settings. We present a strategy for efficient and precise repair of RDEB-associated mutations in the *COL7A1* gene. We compared the efficacy of double-strand breaks (induced by CRISPR/Cas9), single nicks, or double nicks (induced by Cas9n) in mediating repair of a *COL7A1* splice-site mutation in exon 3 by homologous recombination (HR). We accomplished remarkably high HR frequencies of 89% with double nicking while at the same time keeping unwanted repair outcomes, such as non-homologous end joining (NHEJ), at a minimum (11%). We also investigated the effects of subtle differences in repair template design on HR rates and found that strategic template-nicking can enhance *COL7A1*-editing efficiency. In RDEB patient keratinocytes, application of double-nicking led to restoration and subsequent secretion of type VII collagen at high efficiency. Comprehensive analysis of 25 putative off-target sites revealed no off-target activity for double-nicking, while usage of Cas9 resulted in 54% modified alleles at one site. Taken together, our work provides a framework for efficient, precise, and safe repair of *COL7A1*, which lies at the heart of a future curative therapy of RDEB.

INTRODUCTION

Recessive dystrophic epidermolysis bullosa (RDEB) is a devastating inherited skin disease that causes severe blistering of the skin and mucous membranes upon minor mechanical stress. RDEB is caused by loss-of-function mutations in the anchoring filaments forming *COL7A1*. The severity of RDEB depends on the type of the mutation and its location within the *COL7A1* (NCBI Nucleotide: NM_000094) gene.[1] RDEB is typically associated with additional severe clinical complications like aggressive squamous cell carcinoma that arise in early adulthood and are the main cause of mortality in these patients.[2] So far, clinical approaches to treat RDEB mainly focus on ameliorating the symptoms rather than a cure of the disease. Different therapeutic strategies for reverting the loss of *COL7A1* have been envisioned and applied, with varying success, in clinical studies.[3–6] Gene therapy, using retro- or lentiviral vectors for reconstitution of functional *COL7A1* in keratinocytes or fibroblasts, is a promising candidate curative therapy but appears to face several severe obstacles. These include low transduction efficiencies due to the large size of *COL7A1* (cDNA 9.3 kb), random integration of the transgene flanked by viral sequences, and unwanted recombination of repetitive gene regions.[4,7]

Direct gene-editing of mutant patient cells, potentially even *in vivo*, is a highly attractive avenue. The introduction of powerful CRISPR/Cas-based technologies has significantly boosted the popularity of gene editing. Moreover, gene-editing offers the possibility to treat dominant-negative forms of the disease that are eluding conventional gene replacement strategies. The first bacterial CRISPR system to be repurposed for gene editing in human cells was the type II system from *Streptococcus pyogenes*.[8,9] Since its inception, the CRISPR gene-editing toolbox has gone through a dramatic expansion, including the discovery of other targeting nucleases, most prominently Cas12a,[10] the repurposing of *Streptococcus pyogenes* Cas9 (from here on Cas9) for transcriptional modulation,[11] or the development of high-fidelity versions of Cas9 for improved targeting precision.[12]

Precise, sequence-specific editing relies on simultaneous delivery of a single-guide RNA (sgRNA) and the targeting Cas nuclease.[13] CRISPR/Cas-mediated site-specific DNA cleavage activates endogenous cell DNA-repair pathways. Depending on cell type, cell-cycle stage, and

Received 22 August 2019; accepted 12 September 2019;
https://doi.org/10.1016/j.omtn.2019.09.011.

[3]These authors contributed equally to this work.

Correspondence: Ulrich Koller, EB House Austria, Research Program for Molecular Therapy of Genodermatoses, Department of Dermatology, University Hospital of the Paracelsus Medical University Salzburg, Strubergasse 22, 5020 Salzburg, Austria.
E-mail: u.koller@salk.at

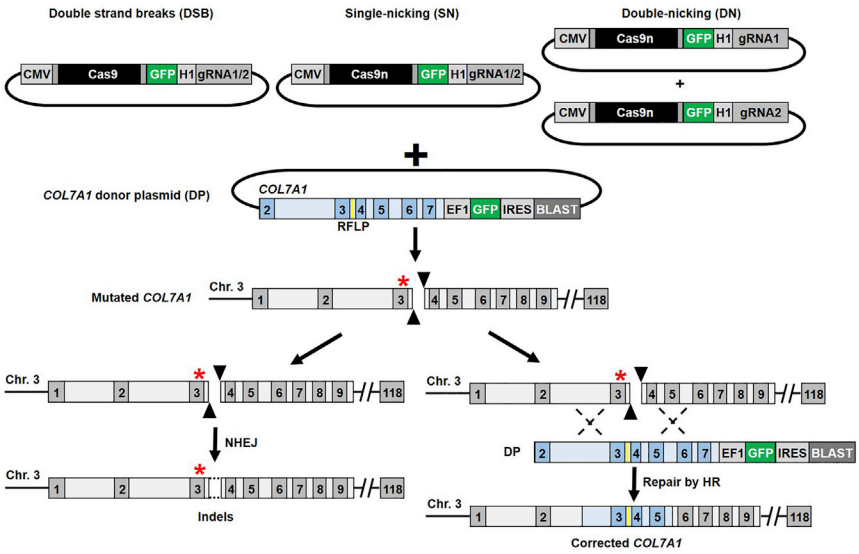

Figure 1. General Strategy for Precise Correction of Splice Site Mutation c.425A > G in Exon 3 of *COL7A1*

Co-transfection of plasmids encoding combinations of Cas9/sgRNA (Cas9/sgRNA1, Cas9/sgRNA2, Cas9n/sgRNA1, Cas9n/sgRNA2, or Cas9n/sgRNA1 and 2) and *COL7A1* DP into RDEB patient keratinocytes leads to the induction of single-strand breaks (SSBs) or double-strand breaks (DSBs) within intron 3 of the *COL7A1* target locus on chromosome 3 (solid arrow heads). The mutation (c.425A > G) at the target locus is indicated with a red asterisk. Consecutive exons and introns of the *COL7A1* gene are represented as dark gray or light gray boxes, respectively. The DP carries wild-type *COL7A1* homology arms ranging from exon 2 to intron 7 (stylized as dark and light blue boxes) for HR, a restriction fragment length polymorphism (RFLP, yellow bar) within intron 3, and a GFP-IRES-blasticidin expression cassette under the control of an EF1 promoter. Generation of SSBs or DSBs leads to activation of cellular repair mechanisms and the induction of insertions or deletions (indels) by NHEJ or precise repair by HR between homologous sequences of mutated and wild-type *COL7A1*. As a result, the disease-associated mutation is corrected, and the RFLP is integrated into the target site. Design strategies and sequences for sgRNAs used in this study can be found in Figure S1.

the presence or absence of a homologous repair template, this may result in non-homologous end joining (NHEJ) or homologous recombination (HR).[13] NHEJ leads to the formation of insertions or deletions (indels) and usually does not lead to correction of the mutated allele. In contrast, HR can lead to precise correction of mutations and is thus highly preferable. A caveat, however, is the generally low efficiency of HR compared to NHEJ. Another concern are putative off-target cleavage activities of Cas9. Although off-target activity of Cas9 is generally considered manageable,[14] concerns about unwanted modifications should be considered in future clinical applications.

Different approaches for CRISPR/Cas9-based correction of RDEB have been described,[15–20] but they either suffer from low correction efficiencies or rely on the deletion of exonic sequences. Furthermore, some repair strategies entailed the introduction of short exogenous DNA sequences and can, therefore, not be considered traceless.[16] Clearly, CRISPR/Cas-mediated HR needs optimization in order to achieve precise correction of *COL7A1* mutations at therapeutically relevant efficiencies.

The use of a catalytically modified version of Cas9, Cas9 nickase (Cas9n or D10A), can significantly reduce the risk of undesired off-target mutagenesis.[21–23] Whereas Cas9 generates blunt DNA double-strand breaks (DSB), Cas9n introduces a single-strand break. In addition, a pair of accordingly designed sgRNAs that positions two nickase molecules in close proximity and in the right orientation allows simultaneous generation of two nicks (staggered DSB) at the target locus. Aside from increased targeting specificity and safety profiles, paired nickases or double-nicking can mediate improved HR outcomes, though efficiency may vary depending on the cell type.[13]

Here, we describe a double-nicking strategy for HR-mediated correction of a splice-site mutation in exon 3 of *COL7A1*. This particular point mutation in exon 3 (c.425A > G) falls into the 5′ splice site and consequently leads to aberrant processing of exon 3. The ensuing production of faulty mRNAs leads to a shift of the open reading frame and generation of premature termination codons.[24] We compared HR efficiencies mediated by Cas9, single-nicking, or double-nicking approaches and found that double-nicking consistently outperforms all other approaches. We also investigated the effects of subtle template modifications and determined that strategic nicking of templates can further improve HR efficiencies. Next-generation sequencing (NGS) of potential off-target regions revealed no detectable nickase-mediated genome toxicity, underscoring the higher safety of using Cas9n compared to Cas9.

In conclusion, our work lays the foundation for efficient, safe, and precise correction of *COL7A1* mutations in RDEB.

RESULTS

Selection and Functional Validation of Specific sgRNA Pairs for HR-Mediated Correction of COL7A1

Initially, we sought to compare gene-editing characteristics (NHEJ versus HR) of Cas9 and Cas9n. The use of a Cas9n in combination with paired sgRNAs was described previously as an appealing strategy for efficient gene-editing with reduced off-target activity.[22,23] Co-delivery of plasmids encoding Cas9 or Cas9n with a donor plasmid (DP) carrying the homologous *COL7A1* sequence for HR is predicted to lead to DNA cleavage at the *COL7A1* target locus and subsequent DNA repair (Figure 1). Upon DNA cleavage, two distinct repair pathways, HR and NHEJ, can be initiated. Whereas HR can lead to precise repair of the mutation, NHEJ generally leads to induction of indels that do not correct the mutation. The desired outcome is that the

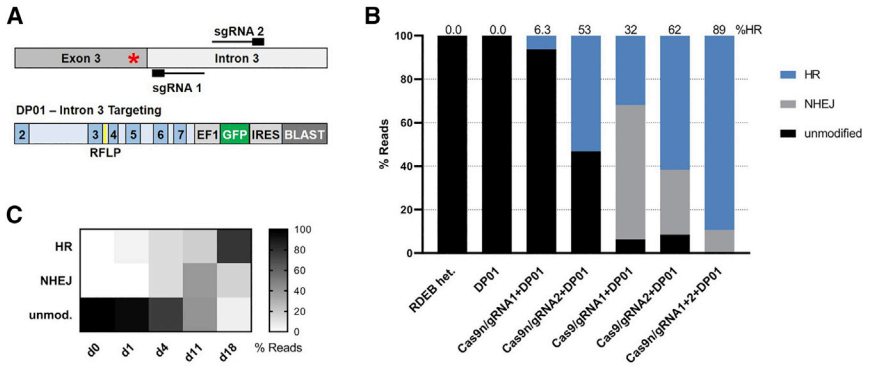

Figure 2. Quantification of Editing Outcomes in CRISPR/Cas9-Treated RDEB Keratinocytes

(A) Schematic depiction of sgRNAs and the DP01 used for intron 3 targeting. The splice-site mutation (c.425A > G) in exon 3 is indicated by a red asterisk, and sgRNA binding sites in intron 3 are shown. The donor plasmid includes wild-type *COL7A1* homology arms spanning exon 2 to intron 7 and features a RFLP (yellow bar) within intron 3 for detection of HR. Consecutive *COL7A1* exons and introns are represented as dark blue or light blue boxes, respectively. (B) Quantitative comparison of HR and NHEJ efficiencies induced by select Cas9/sgRNA and Cas9n/sgRNA combinations. RDEB keratinocytes heterozygous for the splice-site mutation (RDEB het.) were co-transfected with indicated combinations of Cas9/sgRNA (Cas9/sgRNA1, Cas9/sgRNA2, Cas9n/sgRNA1, Cas9n/sgRNA2, or both Cas9n/sgRNA1 and 2) and DP01. Untransfected, non-selected RDEB het. keratinocytes served as negative controls. As a second negative control, RDEB het. keratinocytes were transfected with DP01 only and blasticidin selected for 2 weeks. Genomic sequences were analyzed by PCR amplification of the *COL7A1* on-target locus, sub-cloning, and Sanger sequencing after 2 weeks of blasticidin selection (18 days post-transfection), and relative amounts of repair (HR or NHEJ) are shown. Relative amounts of HR are indicated in dark blue (%HR). (C) Gene-editing kinetics in patient keratinocytes. RDEB het. keratinocytes were co-transfected with Cas9n/sgRNA1 and 2 along with DP01 for *COL7A1* intron 3 targeting. Induction of NHEJ and HR was quantified by PCR amplification of the *COL7A1* on-target locus, sub-cloning, and Sanger sequencing 1 day, 4 days (2 days blasticidin selection), 11 days (9 days blasticidin selection), and 18 days post-transfection (16 days blasticidin selection), respectively. Percentages of gene-editing outcomes are shown in Tables S3 and S4.

presence of a DP will direct HR-mediated repair of the disease-associated mutation and insertion of a restriction fragment length polymorphism (RFLP) into the respective target site (Figure 1). Aiming for specific correction of a recessively inherited splice site mutation (c.425A > G, p.K142R) within exon 3 of *COL7A1* by HR-based repair, we initially predicted putative sgRNA pairs for DNA DSB generation at the target locus using the CHOPCHOP software[25,26] (Figure S1). Promising sgRNA pairs for double-nicking in intron 3 (sgRNA1 and 2) and exon 3 (sgRNA3, 4, and 5) of *COL7A1* were selected according to Ran et al.,[22] featuring a short offset sequence between the sgRNA binding sites (+3 bp to +10 bp) and close proximity of the cleavage site to the mutation (Figure S1). The mutation (c.425A > G) creates an additional protospacer-adjacent motif (PAM) on the mutant allele, which is not present on the wild-type sequence of *COL7A1*, providing the opportunity to include a potentially allele-specific sgRNA (sgRNA4) (Figure S1).

We first assured proper function of different sgRNAs by delivering combinations of plasmids encoding Cas9/sgRNA or Cas9n/sgRNA into HEK293 cells and performing a T7 endonuclease I (T7EI) assay on the PCR-amplified *COL7A1* on-target region (Figure S2). T7EI digestions confirmed that all selected sgRNAs direct Cas9 to the *COL7A1* target region for DSB induction (Figures S2A and S2B). When co-delivering sgRNA1 and 2, sgRNA3 and 4, or sgRNA3 and 5 in combination with Cas9n into HEK293 cells (double-nicking approach), we observed comparable levels of T7EI-mediated cleavage (Figures S2A and S2B). As expected, HEK293 cells transfected with respective Cas9n/sgRNA plasmids (single-nicking) did not show any digestion pattern upon T7EI treatment (Figures S2A and S2B). Although sgRNA4 was expected to exclusively direct the cleavage of mutant *COL7A1*, it also directed the cleavage of wild-type *COL7A1* by Cas9 in HEK293 cells, most likely based on usage of an alternative PAM (NAG instead of NGG) (Figure S2B). An alternative explanation may be that a bulge might allow sgRNA4 to cut wild-type *COL7A1*.[27] The unspecific band in Figure S2B most likely is the result of heteroduplex formation during the initial PCR.[28]

HR-Mediated COL7A1 Repair Using Double-Nicking and Donor Plasmids

For HR-mediated correction of the causal splice-site mutation (c.425A > G) in immortalized RDEB keratinocytes, either heterozygous (RDEB het.) or homozygous (RDEB hom.) for the respective mutation, we first used a DP that carries a homologous donor sequence ranging from exon 2 to intron 7 of *COL7A1*, an EcoRI restriction site within intron 3, elongation factor 1 (EF1)-GFP, and an internal ribosomal entry site (IRES)-blasticidin selection cassette (DP01) (Figure 2A).

We first tested the feasibility of our double-nicking approach by co-transfection of DP01 and a combination of intron 3-specific Cas9n/sgRNA1 and Cas9n/sgRNA2 expression plasmids into immortalized wild-type keratinocytes (hKcs). After 2 weeks of blasticidin selection, we observed almost 100% GFP^+ cells (Figure S3A), which were further analyzed regarding gene-editing efficiency. To this end, we performed a nested PCR on the *COL7A1* on-target region. Subsequent EcoRI digestion of the resulting PCR products indicated high HR efficiency (Figures S3B and S3C). Untransfected hKcs served as negative controls.

Next, we tested our constructs in RDEB het. keratinocytes and compared Cas9, Cas9n single-nicking, and double-nicking in directing HR-mediated repair of *COL7A1*. Untransfected RDEB het. keratinocytes (no antibiotic selection) and RDEB het. keratinocytes transfected with DP01 only (blasticidin-selected) served as negative controls. To exclude the potential impact of variable transfection

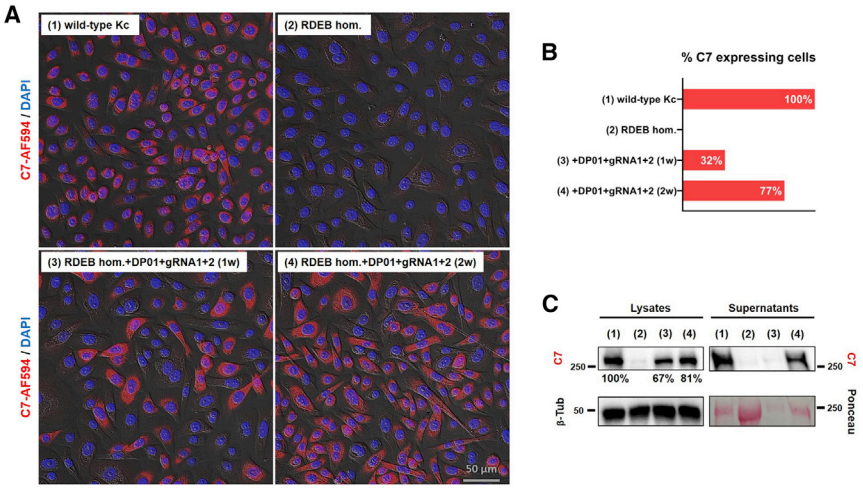

Figure 3. Precise Repair by HR Restores C7 Expression in RDEB Keratinocytes

Delivery of intron 3-specific Cas9n/sgRNA (sgRNA 1+2) in combination with DP01 into RDEB keratinocytes (RDEB hom.) with a homozygous splice-site mutation in exon 3 (c.425A > G, p.K142R) led to HR-mediated repair of the mutation. (A) C7 immunofluorescence (IF) staining of wild-type keratinocytes (wild-type Kc, top left) and treated RDEB keratinocytes revealed restoration of comparable levels of C7 after 1 (1w, bottom left) and 2 weeks of blasticidin selection (2w, bottom right). Untreated RDEB keratinocytes (RDEB hom., top right) lacking detectable C7 expression served as negative control. (B) Quantification of $C7^+$ cells by cell counting (886 cells/sample on average). Percentages of $C7^+$ cells are indicated. (C) Western blot analysis of cell lysates and cell culture supernatants form treated RDEB hom. keratinocytes. Proteins were revealed using antibodies against C7 and β-tubulin (β-tub). Wild-type keratinocytes and untreated RDEB hom. keratinocytes served as positive and negative control, respectively. Densiometric analysis of the C7 bands was performed, and relative values are indicated. Numbering of lanes ([1], [2], [3], and [4]) corresponds to sample descriptions in (A) and (B).

efficiencies and to maintain a homogeneous cell population harboring the transfected plasmids, the target cell population was pre-selected with blasticidin. In general, we achieved a transfection efficiency of ~30% in immortalized RDEB het. keratinocytes as estimated by the analysis of GFP expression via flow cytometry (Figure S4A). As expected, following 2 weeks of blasticidin selection, ~99% of RDEB het. keratinocytes were GFP^+ (Figure S4B).

At this point, cells were harvested, genomic DNA was extracted, and the target region was PCR-amplified using a primer pair binding to intron 1 and exon 5 of *COL7A1*, thereby excluding possible amplification of persisting DP (Table S2). A nested PCR was performed, and fragments were sub-cloned and analyzed by Sanger sequencing. Highest HR efficiency (89%) was found in cells treated with Cas9n/sgRNA1 and sgRNA2 in a double-nicking configuration (Figure 2B). Indel formation via NHEJ was observed in 11% of analyzed clones, whereas an increased occurrence of NHEJ was detectable with Cas9/sgRNA1 (62%) and Cas9/sgRNA2 (30%) (Figure 2B). Co-transfection of DP01 together with either Cas9n/sgRNA1 or Cas9n/sgRNA2 expression plasmids only resulted in the HR-mediated integration of the EcoRI restriction site at the target locus without any detectable indels. 6% HR was achieved with Cas9n/sgRNA1 and remarkable 53% with Cas9n/sgRNA2 (Figure 2B).

We also compared HR efficiencies induced by intron 3 targeting sgRNAs (sgRNA1, sgRNA2) to those induced by combinations of sgRNAs targeting exon 3 (sgRNA3, sgRNA4, sgRNA5). We found that sgRNAs targeting exon 3 were slightly less efficient in inducing HR. Specifically, HR efficiencies of 63% (Cas9n/sgRNA3 and Cas9n/sgRNA4) and 80% (Cas9n/sgRNA3 and Cas9n/sgRNA5) were observed for the sgRNA combinations targeting exon 3 (Figure S5C).

Kinetic studies in RDEB het. keratinocytes treated with intron 3-specific double-nicking constructs (Cas9n/sgRNA1 and 2) and DP01 highlighted the impact of blasticidin selection on general HR efficiency. One day after transfection, HR was already detectable at about 5%, but increased to almost 13% 4 days after treatment and 2 days of selection (Figure 2C). We assume that at this point, nearly all cells harbored the DP01 due to selection pressure. Eleven days after transfection and 9 days of blasticidin selection, NHEJ was detected in 40% of all analyzed sequences and was, therefore, still more prominent than HR, which increased to 19%. After 2 weeks of selection, however, HR efficiency increased to 78%, whereas NHEJ decreased to 16% (Figure 2C). To test whether the increase in HR efficiency is due to persisting Cas9 expression in bulk-selected cells, Cas9 protein levels were monitored at different time points after transfection into RDEB het. keratinocytes by western blot analysis. As expected, Cas9 expression levels significantly decreased within the first 7 days after transfection (Figure S6).

Restoration of Type VII Collagen Expression in RDEB Keratinocytes

To test if HR-meditated repair of *COL7A1* correlated with restoration of type VII collagen (C7) expression in RDEB keratinocytes, we transfected the intron 3-specific Cas9n/sgRNA combination (sgRNA1+2) (Figure 2A) along with DP01 into an immortalized RDEB hom. keratinocyte cell line. Ensuing DNA cleavage and precise HR between DP01 and endogenous *COL7A1* led to the correction of the mutation and thus to restoration of C7 expression in treated cells, as shown by immunofluorescence microscopy (Figure 3A). No C7 expression was detectable in untreated RDEB keratinocytes. Quantification of C7-expressing cells by cell counting revealed an encouraging 32% and 77% of $C7^+$ cells after 1 and 2 weeks of blasticidin selection, respectively (Figure 3B). The percentages are in good accordance with our genomic analysis of HR efficiencies described above.

Western blot analysis of cell lysates and cell culture supernatants further supported restoration of functional C7. We observed increasing

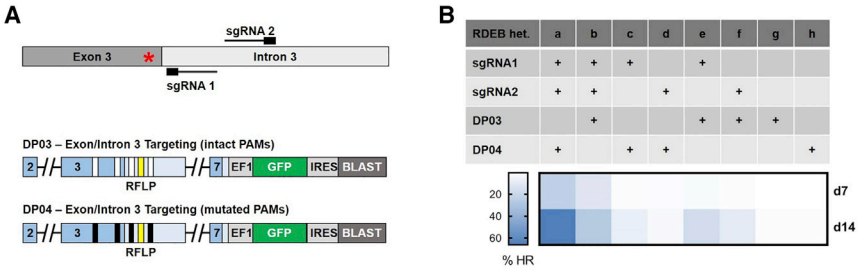

Figure 4. Donor Templates Design for Improved HR Efficiencies in RDEB Keratinocytes

(A) Schematic depiction of intron 3-targeting sgRNA binding sites relative to splice-site mutation c.425A > G (red asterisk) and design of modified DPs, DP03 and DP04. *COL7A1* homology arms are depicted as blue boxes, and locations of PAMs are indicated. White bars indicate intact PAMs (DP03), and black bars correspond to mutated PAMs. An RFLP (yellow bar) within intron 3 was included for detection of HR. (B) Transfection scheme and NGS quantification of HR efficiencies in RDEB patient keratinocytes heterozygous for splice site mutation (RDEB het.). Combinations of Cas9n/sgRNA-encoding plasmids were delivered with indicated DPs (DP03 or DP04). HR efficiencies were analyzed after 7 and 14 days of blasticidin selection and are presented as heatmaps (dark blue colors correspond to higher HR efficiencies). Percentages of gene-editing outcomes are shown in Table S5.

levels of full-length C7 in lysates and supernatants of RDEB hom. keratinocytes treated with DP01+sgRNA1+2 after 1 and 2 weeks of selection (Figure 3C). Quantification of C7 signals showed that, after 2 weeks of selection, expression levels of reconstituted C7 were nearly comparable (81%) to those of wild-type keratinocytes (100%, respectively) (Figure 3C).

Of note, HR efficiency calculated by the presence of an RFLP (present in 89% of alleles after 2 weeks of selection; see Figure 2B) was slightly above the values we found when quantifying reconstituted full-length C7 by immunofluorescence (77% $C7^+$ cells after 2 weeks of selection). We recognized that the difference could be due to targeted or random integration of the entire DP or parts thereof. We devised a PCR-based strategy to discriminate between HR events leading to restoration of full-length C7 expression and those leading to targeted integration of the DP backbone. Importantly, random integration, or persisting plasmid, would not be amplified by our PCR strategy and, therefore, not falsely be quantified as HR (Figure S7). Although we found that targeted integration of parts of the DP backbone do actually occur, those events constitute only a minority of all HR events.

Impact of PAM Inactivation on General HR Efficiency

Next, we investigated whether inactivation of the respective PAMs within the donor sequence influences HR efficiencies in RDEB het. patient keratinocytes. To this end, we designed a DP03 featuring the endogenous target sequences (intact PAMs) and compared it to a DP harboring inactivated PAM sequences on both homology arms (DP04) (Figure 4A). In addition, we compared HR efficiencies induced by single- and double-nicking. As expected, after 14 days of selection, double nicking induced significantly higher HR rates (66% for DP04 and 27% for DP03) and increased conversion of mutant to wild-type *COL7A1* alleles (data not shown) compared to single-nicking (HR rates, 8% and 2% for DP04; 17% and 10% for DP03). Importantly, inactivation of the PAM sequences in the DP (DP04) enhanced the HR efficiency from 27% up to 66% for intron 3 targeting (Figure 4B). Similar HR efficiencies (63%) were achieved using exon 3-targeting double-nicking (Figure S8).

Paired Double-Nicking Improves HR Efficiencies

Recently, Chen et al.[29] showed that flanking the homologous donor sequence with additional Cas9n target sites (TSs, including the PAMs) can further improve knockin (HR) efficiencies in pluripotent stem cells. Therefore, we designed different DPs (DP05-12) with inactivated PAM sites within the homologous arms and added different constellations of flanking sgRNA TSs (TS3 or TS4/5) (Figure S9A). We co-transfected a total of nine different DPs together with Cas9n/sgRNA5, Cas9n/sgRNA3, or Cas9n/sgRNA3+5-expressing plasmids (Figure S9B) into RDEB het. patient keratinocytes and started blasticidin selection 2 days post-transfection for 2, 5, and 10 days, each. Analogous to the findings of Chen et al.,[29] we observed increased HR efficiencies for paired nicking (samples e–g and i–k) with up to 9% HR rate compared to single-nicking (Figure S9C, samples d and h), with up to 1.6% HR rate after 10 days of selection. In addition, on-target double-nicking induced significantly higher HR rates in general (samples a–c, up to 25.5% HR rate) compared to the single-nicking samples (samples d–k, up to 9% HR rate). Double-nicking in combination with donor template double-nicking (paired double-nicking, samples b and c) additionally improved HR rates from 18% up to 25.5% after 10 days of selection (Figure S9C).

To assess whether one flanking or two flanking TSs are required for improved HR efficiencies upon double-nicking, we co-transfected all different DPs (DP02, DP05–12) together with the Cas9n/sgRNA3+5 pair into RDEB het. patient keratinocytes and selected them 2 days after transfection for 1 week with blasticidin. NGS analysis revealed improved HR rates (8% up to 11%) for all samples treated with repair templates containing flanking TSs (DP05–DP12) compared to HR (5%) achieved with the original donor template (DP02). The most efficient repair templates showed an HR increase of up to 2-fold at the genomic level (Figure S10A).

Finally, we co-transfected all generated DPs along with the Cas9n/sgRNA3+5 pair (double-nicking) into the RDEB hom. patient keratinocyte cell line to ascertain that HR rates observed by NGS correlate with correction and restoration of C7 protein. We started blasticidin selection of treated bulk populations 2 days post-transfection for 5 days and analyzed restoration of C7 expression via immunofluorescence microscopy. Our immunofluorescence data confirmed NGS

Table 1. Predicted Off-Target Regions within the Human Genome

Name	Bulge Type	Target Site	PAM	Chr.	Position	Dir.	Mism.	Bulge Size
sgRNA1	X	DNA: 5′-TGGGAGGCATGGTAGGGGTGGG-3′	GGG	Chr.3	48593508	+	0	0
OT1	X	DNA: 5′-gGGGtGGgATGGTAGGGGTAGGG-3′	GGG	Chr.7	128066174	–	3	0
OT2	X	DNA: 5′-TGaGAGtaATGGTAGGGGTAAGG-3′	AGG	Chr.6	115600821	+	3	0
OT3	X	DNA: 5′-TGGGAGGCATGGaAGGGGTcGAG-3′	GAG	Chr.2	27052009	–	2	0
OT4	X	DNA: 5′-TGtGAGaCAgGGTAGGGGTAGAG-3′	GAG	Chr.12	103181813	–	3	0
OT5	X	DNA: 5′-TGGGAaGaATGGgAGGGGTAGAG	GAG	Chr.7	49864974	+	3	0
OT6	X	DNA: 5′-TGGaAGGCAaaGTAGGGGTAAAG-3′	AAG	Chr.15	69867776	–	3	0
OT7	X	DNA: 5′-TGGGAGaCATGcaAGGGGTAAAG-3′	AAG	Chr.17	53017784	–	3	0
OT8	X	DNA: 5′-TGGGtGGCAgGGaAGGGGTAGAG	GAG	Chr.6	143390635	–	3	0
OT9	RNA	DNA: T-5′-GGAGGCATGGTAaGGGTAAGG-3′	AGG	Chr.7	49312556	+	1	1
OT10	RNA	DNA: 5′-TGtGAGGCA-GGTAGGGGTAGGG-3′	GGG	Chr.16	57993429	+	1	1
OT11	DNA	DNA: 5′-TGGGAGGCAgGGTAGG+GGTAAAG-3′	AAG	Chr.20	18188729	–	1	1
OT12	RNA	DNA: 5′-TGGGAGcCATGG-AGGGGTAAGG-3′	AGG	Chr.19	4567778	–	1	1
sgRNA2	X	DNA: 5′-TGACCCCAAATGAAGTGTCCAGG-3′	AGG	Chr.3	48593482	–	0	0
OT1	X	DNA: 5′-TcACCtaAAATGAAGTGTCCTGG-3′	TGG	Chr.4	148479916	+	3	0
OT2	X	DNA: 5′-TGgCCCCAAgTGAAcTGTCCGGG-3′	GGG	Chr.7	151453441	–	3	0
OT3	X	DNA: 5′-TGAtCCCAAATGAAGTcTCaTGG-3′	TGG	Chr.4	102038476	+	3	0
OT4	X	DNA: 5′-TGAtCCCAtATGAAGgGTCCGAG-3′	GAG	Chr.14	91551068	–	3	0
OT5	DNA	DNA: 5′-TGACCtCAAATGAAG+TGTCCAGG	AGG	Chr.5	41656495	–	1	1
OT6	RNA	DNA: 5′-TG-ggCCAAATGAAGTGTCCTGG-3′	TGG	Chr.8	101719126	+	2	1
OT7	RNA	DNA: TGAtCCCAAATG-tGTGTCCTGG-3′	TGG	Chr.7	67323816	–	2	1
OT8	RNA	DNA: 5′-TGACCCCAcATaAAGT-TCCAGG-3′	AGG	Chr.4	176645058	–	2	1
OT9	RNA	DNA: 5′-TG-CCaCcAATGAAGTGTCCCGG-3′	CGG	Chr.13	112202093	+	2	1
OT10	RNA	DNA: 5′-TGACCCCAAcaG-AGTGTCCCGG-3′	CGG	Chr.19	17264712	–	2	1
OT11	RNA	DNA: 5′-TGA-CtCAAAgGAAGTGTCCAGG-3′	AGG	Chr.14	75842876	–	2	1
OT12	DNA	DNA: 5′-TGACCCCAtATGAAGTGTC+CTAG-3′	TAG	Chr.X	53596749	–	1	1
OT13	RNA	DNA: 5′-TGACaCCAAAT-AAGTGTCCAAG-3′	AAG	Chr.10	113212645	+	1	1
OT14	RNA	DNA: 5′-TGACCCCAcATG-AGTGTCCCAG-3′	CAG	Chr.X	89008746	–	1	1

Chr., Chromosome; Dir., Direction; Mism., Mismatches.

results, showing that the addition of TSs flanking the homologous arms on the repair templates can further improve HR efficiency, resulting in the correction of the targeted mutation and thereby restoring C7 in treated patient keratinocytes (Figures S10B and S10C).

Off-Target Analysis Reveals Superior Safety Profile of Double-Nicking Approach

Future clinical implementation of gene-editing therapies needs to address safety concerns originating from potential off-target activity of Cas9. RNA-guided engineered nucleases not only cleave on-target sites but may also cleave off-target sites that differ by several nucleotides from the on-target sites, causing unwanted off-target mutations. Cas9 originated from *Streptococcus pyogenes* recognizes 5′-NGG-3′ PAM sequences but also, to a lesser extent, 5′-NRG-3′. In addition, Lin et al.[27] could show that CRISPR/Cas9 systems can tolerate an extra base (DNA bulge) or a missing base (sgRNA bulge) at various locations compared with the corresponding RNA guide strand. We predicted several different off-target loci using the CRISPR RGEN tool (Cas-OFFinder) (http://www.rgenome.net/cas-offinder/)[30] and performed NGS on genomic DNA isolated from Cas9/sgRNA1, Cas9/sgRNA2, and Cas9n/sgRNA1+2-treated and blasticidin-selected RDEB het. keratinocyte bulk populations. We analyzed 26 different sgRNA off-target sites, 12 for sgRNA1 and 14 for sgRNA2 (Table 1), and compared the off-target activity of Cas9 and Cas9n. NGS analysis revealed considerable off-target activity of Cas9 and the induction of deletions at the sgRNA1 off-target locus 9 (OT9) (Figure 5A). Importantly, no such off-target activity was detected in cells treated with Cas9n, emphasizing the improved safety profile of double-nicking (Figure 5A). We confirmed our NGS findings by performing a T7EI assay on the PCR-amplified OT9 (Figure 5B). Analysis of the deletion profile at OT9 revealed the prevalence of certain deletions, which account for more than 80% of all observed modifications (Figure 5C).

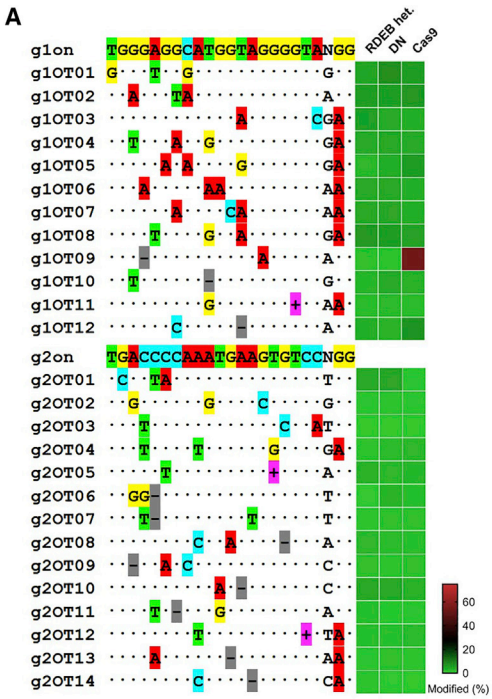

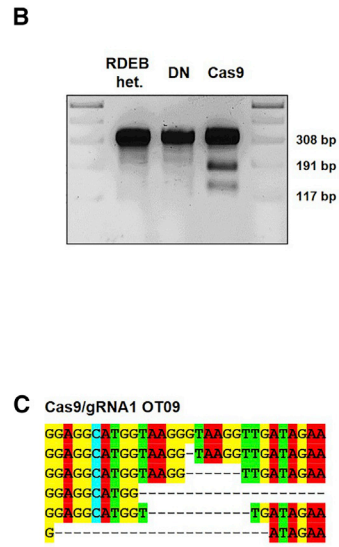

Figure 5. Safety Profile of *COL7A1* Intron 3-Targeting sgRNAs

(A) Off-target (OT) sites for *COL7A1* intron 3-targeting sgRNAs 1 and 2 (g1, g2) were predicted with Cas-OFFinder and mismatches relative to the on-target (on) site are shown with colored boxes. Gray boxes (–) correspond to RNA bulges, and purple boxes (+) indicate DNA bulges. Indel frequencies as detected by targeted amplicon NGS sequencing are presented as heatmaps. Each off-target site was amplified from RDEB patient keratinocytes (heterozygous for splice site mutation c.425A > G) treated with Cas9n (DN) or Cas9. Untreated RDEB keratinocytes (RDEB het.) served as control. Genomic loci for all off-target sites can be found in Table 1. (B) Verification of targeted amplicon sequencing by T7EI assay. 2 weeks after selection, genomic DNA was isolated from cells treated with Cas9n (DN) or Cas9, and PCR was performed on OT09. Genomic DNA from untreated cells served as negative control (RDEB het.). (C) Schematic depiction of main deletions observed at sgRNA1 off-target site 9 (OT09). The indicated sequences account for more than 80% of all deletions observed by targeted amplicon sequencing.

DISCUSSION

In the work presented here, we describe an improved selection-based strategy for highly efficient repair of RDEB-associated mutations in *COL7A1*. Specifically, we compared the efficiencies of DSBs (induced by Cas9), single nicks, or double nicks (induced by Cas9n) in driving HR-mediated repair of *COL7A1* (c.425A > G splice-site mutation in exon 3) and found that double-nicking consistently yields superior repair outcomes.

For double-nicking, we tested exon- as well as intron-targeting pairs of sgRNAs and found comparable HR efficiencies. Considering the lower risk of inducing unwanted open reading frame mutations, we opted for the intron-targeting pair of sgRNAs in subsequent experiments. After 2 weeks of antibiotic selection, we found remarkable HR efficiencies of up to 89%. Importantly, only about 11% of all analyzed clones displayed signs of undesired NHEJ (indels). In RDEB patient keratinocytes homozygous for the splice-site mutation, application of our double-nicking strategy led to restoration of C7 expression at high efficiency. A potential caveat of using intron-specific sgRNAs might be the increased frequency of single nucleotide polymorphisms (SNPs) in patient introns that demands careful consideration during sgRNA design.

A significant concern is that our selection-based strategy may lead to targeted or random integration of the entire DP or large parts thereof, thereby skewing the accurate measurement of HR efficiency. Indeed, we obtained data that point to the existence of targeted integration of parts of the DP, including the DP backbone. However, ensuing semi-quantitative experiments indicate that only a minority of HR events are actually due to targeted integration of large portions of the DP (Figure S7). On the other hand, random integration or persisting plasmid would not be amplified by our PCR strategy and, therefore, not falsely be quantified as HR. Although our selection-based system demands careful interpretation of absolute HR efficiencies, we believe that it is an excellent system for directly comparing different DSB, single-nicking, and double-nicking strategies in driving HR and precise repair of disease-causing mutations. Our results, consequently, provide a rationale for further development of the double-nicking strategy.

In addition, we evaluated the safety of our *COL7A1* intron 3 double-nicking strategy by NGS analysis. We investigated off-target activities of Cas9 and Cas9n at 26 different predicted sites and found pronounced Cas9-induced modifications at one locus (OT9). At this site, Cas9 allowed one RNA bulge and one mismatch, compared to the sgRNA1 on-target region for cutting. Importantly, no off-target activity was detectable at any site for Cas9n double-nicking.

A variety of strategies have been tried or envisioned to ease the burden of the RDEB,[31] but a complete cure remains an ambitious future goal. The ability to genetically modify patient cells with high efficiency is a critical prerequisite toward this goal. Although the most desirable treatment option for RDEB, and many other inherited diseases for that matter, is correction of causative mutations *in vivo*, strategies toward this end are still far from application in clinical settings. Concerns regarding efficient and safe delivery of gene-editing reagents still persist. Consequently, cutaneous *ex vivo* gene therapy, the transplantation of genetically modified keratinocyte stem cells, remains at the center of RDEB research up to this date.

In general, *ex vivo* gene therapy relies on either gene replacement, where a full copy of the wild-type gene is introduced into patient-derived cells, or gene-editing, where the mutated gene is reverted to wild-type by DNA-modifying reagents, such as CRISPR/Cas9. Whereas gene replacement approaches have been successful for other forms of EB, such as the substitution of *LAMB3* in cells from patients with junctional epidermolysis bullosa,[32–34] efforts to replace mutant *COL7A1* in cells from RDEB patients have yielded limited therapeutic applicability so far.

Several groups successfully attempted gene-editing of *COL7A1* in cells derived from RDEB patients.[15–20,35] Chamorro et al.[35] introduced a transcription activator-like effector nuclease (TALEN)-based strategy for correction of the c.6527insC mutation in *COL7A1*. They combined adeno-associated virus (AAV)-mediated delivery of repair template with adenovirus (AV)-mediated delivery of TALENs and observed restoration of the *COL7A1* reading frame by both HR and NHEJ in clones of keratinocytes.[35]

Other approaches used the combination of gene-editing and induced pluripotent stem cell (iPSC) technologies as a potential treatment of RDEB.[15] Here, patient-derived primary fibroblasts were initially modified and subsequently used to obtain iPSCs. These iPSCs were later re-differentiated into different cells types, including keratinocytes. Owing to low editing efficiency, the protocol included an antibiotic selection step of cells in bulk, limited dilution, clonal selection, single-cell expansion, and screening of individual clones. For antibiotic selection, a puromycin cassette flanked by loxP sites was employed that, after Cre-mediated removal, leaves a loxP footprint in the targeted intron.

For dominant-negative mutations, reading-frame disruption offers an interesting alternative to HR-based approaches. Shinkuma et al.[36] targeted the c.8068_8084delinsGA mutation in exon 109 of *COL7A1* associated with dominant-negative dystrophic epidermolysis bullosa (DDEB). Mutation site-specific NHEJ was induced by CRISPR/Cas9-based gene-editing in iPSCs generated from patient-derived fibroblasts, leading to knockout of the mutant-specific allele while leaving the wild-type allele intact. A caveat with the approach is the dependence on a complex mutation (17-bp deletion with a GA insert) that allows the design of a mutant allele-specific sgRNA that is absent in the wild-type allele. Furthermore, prediction of repair outcomes was described only recently[37–39] and was, therefore, not considered for sgRNA design. Consequently, only a small number of modified cells showed the desired phenotype of uninterrupted C7 trimer formation.

Clearly, improved HR efficiencies and predictable repair outcomes are pivotal for advancing experimental gene therapies into clinical settings. Based on previous studies, a correction efficiency of 35% is estimated to be sufficient for complete phenotypic recovery *in vitro* and *in vivo*.[40,41] Numerous aspects have an influence on HR efficiencies, including delivery and modus operandi of DNA-modifying agents, the nature of the repair template, or cell type and cell cycle stage. High efficiency, high precision, and seamless repair all need to be carefully balanced in future *ex vivo* therapies to circumvent the need for antibiotic selection and clonal expansion of corrected cells. Although Cas9 is highly efficient in inducing DNA DSBs and ensuing DNA repair, subtle modifications in experimental design can significantly alter the outcome of such efforts. Furthermore, CRISPR/Cas approaches require at this point a transfection of target cells that might alter the proliferative capacity of edited cells. Specifically, keratinocytes might lose their potential to proliferate.

An increasing number of reports describe successful *COL7A1*-editing in immortalized and primary cells.[15–20,35,36,42] We previously described HR-based correction of a *COL7A1* hotspot mutation in exon 80.[16] While NGS analysis revealed an on-target cutting efficiency of up to 30% and no detectable-off-target events, relatively low HR efficiencies made the use of a selection-based system and expansion of corrected single-cells clones mandatory. Consequently, subsequent removal of the selection system left a 116 nucleotide insert at the target locus and could, therefore, not be considered traceless repair.

Recently, Cas9/sgRNA ribonucleoproteins (RNPs) have been shown to provide increased targeting efficiency compared to plasmid transfection.[43] Higher rates of editing and shorter persistence in the nucleus combine for a larger number of edited cells and reduced off-target activity.[44] RNPs have been tested *ex vivo* and *in vivo* for correction of RDEB-associated *COL7A1* mutations in exon 80.[19,42] Excision of exon 80 resulted in restoration of C7 and functional correction in RDEB keratinocytes without noticeable toxicity.[19]

Going forward, we believe that combining RNP delivery with double nicking and optimized repair templates will offer the best option for correction of *COL7A1* mutations in terms of efficiency and precision.

MATERIALS AND METHODS

Design and Cloning of sgRNA Specific for Exon 3 and Intron 3 of COL7A1

Putative sgRNA target sites within exon 3 and intron 3 of the *COL7A1* gene were predicted using the online prediction platform CHOPCHOP.[25,26] sgRNA4 was rationally designed to preferentially target the mutant allele, since the splice-site mutation in exon 3 in the patient cell lines creates a new PAM site not present in human wild-type keratinocytes. sgRNA1 and 2 were designed to target intron 3, while sgRNA3, 4, and 5 were designed to target exon 3 of *COL7A1* and cloned as double-stranded oligonucleotides (Table S1) into either the CMV-T7-hspCas9-T2A-GFP-H1-gRNA CAS740G-1 linearized SmartNuclease vector or the CMV-T7-hspCas9-nickase-T2A-GFP-H1-gRNA CAS790G-1 linearized SmartNickase vector (System Bioscience, Palo Alto, CA, USA) according to the manufacturer's protocol.

Generation of Donor Plasmid (DP01) for Intron 3 Targeting

The *COL7A1* HR DP for intron 3 targeting (sgRNA1 and sgRNA2) was PCR-amplified and cloned into the MN511A-1 vector (System

Bioscience, Palo Alto, CA, USA), harboring an EF1-GFP and an IRES-blasticidin selection cassette integrated via the SalI restriction site. PCR amplification of the 5′ homologous *COL7A1* sequence fragment was performed using genomic DNA from a healthy donor as template. The PCR product was generated using an exon 2-specific forward primer (P11) and an intron 3-specific reverse primer (P12) and subsequently cloned into the MN511A-1-MC vector via SmaI and EcoRI restriction sites. The resulting 1,054-bp PCR fragment includes silent mutations to inactivate the PAM next to the sgRNA1 binding site within intron 3. The second PCR fragment (1,051 bp) was amplified using an intron 3-specific forward primer (P13), including two silent mutations to inactivate the PAM next to the sgRNA2 binding site within intron 3, and an intron 7-specific reverse primer (P14) and was subsequently cloned using the restriction sites EcoRI and BamHI into the target vector. Sanger sequencing confirmed all resulting plasmid sequences. The final homology donor template encompasses the entire *COL7A1* region spanning from exon 2 to intron 7 and includes an EcoRI site within intron 3 for convenient HR detection. The IRES-blasticidin cassette was cloned downstream of an EF1-GFP cassette according to Peking et al.[45] (see Table S1 for primer sequences).

Generation of the Donor Plasmids Harboring Intact (DP03) or Mutated PAM Sites (DP04) for Exon and Intron 3 Targeting

To create DPs with either four intact (DP03) or four mutated PAM sites (DP04), we performed mutagenesis using the Q5 site-directed mutagenesis kit (New England Biolabs, Frankfurt am Main, Germany) according the manufacturer's protocol. Site-directed mutagenesis on the DP for intron 3 targeting, which harbors the inactivated PAM sites for sgRNA1 and sgRNA2, created one repair template with intact PAMs (DP03) and one template with mutated PAMs (DP04) for all five sgRNA binding sites used in our experiments. The resulting homology donor templates encompasses the entire *COL7A1* region spanning from exon 2 to intron 7 and incorporates EcoRI restriction site within intron 3, facilitating HR detection (see Table S1 for primer sequences).

Generation of Different Donor Plasmids Used for Exon 3 Targeting (DP02, DP05–12)

The 5′ and 3′ homologous *COL7A1* arms for exon 3 targeting (sgRNA3, sgRNA4, and sgRNA5) were PCR-amplified and sequentially cloned into the MN511A-1 vector. The 5′ homologous arm (818 bp) was PCR-amplified using an intron 2-specific forward primer (P15) and an exon 3-specific reverse primer (P16) incorporating two silent mutations in exon 3, one resulting in a NheI restriction site and the second resulting in the inactivation of the PAM site next to the sgRNA3 binding site. The PCR fragment was cloned into the MN511A-1 vector via the restriction sites SmaI and NheI. The 3′ homologous arm (868 bp) was PCR-amplified using an exon 3-specific forward primer (P17), which incorporates six silent mutations, five of them preventing binding of sgRNA4 and sgRNA5 and one resulting in a NheI restriction site within exon 3, and an intron 6-specific reverse primer (P18). The resulting PCR fragment was cloned into the 5′ HA containing MN511A-1 vector via NheI and BamHI. Sanger sequencing validated all constructs. The resulting homology donor template (DP02) encompasses the entire *COL7A1* region from intron 2 to intron 6 and incorporates a NheI site within exon 3, thereby not changing the amino acid code and facilitating HR detection.

Subsequently, six different PCR fragments were PCR-amplified from the original donor template (DP02) using either intron 2-specific forward primer (P27, P29), which includes flanking sgRNA3 and sgRNA4 binding sites with intact PAMs, and/or intron 6-specific reverse primer (P28, P30), which includes flanking sgRNA3 and sgRNA4 binding sites with intact PAMs. The resulting PCR fragments were cloned into the MN511A-1 vector via the SmaI and BamHI sites, concurrently excising the cytomegalovirus (CMV) promotor. The resulting homology donor templates (DP05–10) encompass the entire *COL7A1* region spanning from intron 2 to intron 6 and incorporate a NheI site within exon 3 for HR detection. In addition, these donor templates encompass either 5′-flanking TSs for sgRNA3 or sgRNA4, 3′-flanking TSs for sgRNA3 or sgRNA4, or both.

Donor templates (DP11 and DP12) encompassing 5′ and 3′ sgRNA3 TSs or 5′ and 3′ sgRNA4 TSs were created using primers for Q5 mutagenesis and the pre-existing donor templates DP05 and DP07 (see Table S1 for primer sequences).

Transient Transfection of Donor Plasmids

The embryonic kidney cell line HEK293 (Stratagene, La Jolla, CA, USA) was cultivated in DMEM supplemented with 10% fetal bovine serum (FBS) and 100 U/mL penicillin/100 μg/mL streptomycin (Biochrom, Berlin, Germany). RDEB keratinocytes were obtained via skin biopsies of two patients (RDEB16 and RDEB223) carrying a homozygous splice-site mutation in *COL7A1* exon 3 (c.425A > G / c.425A > G) and one patient (RDEB03) carrying combined heterozygous mutations (c.425A > G / c.5440C > T) in exon 3 and exon 63 of *COL7A1*, upon received written informed consent. The immortalized RDEB keratinocyte cell lines were termed RDEB het. and RDEB hom. throughout the manuscript. Immortalized RDEB keratinocytes and normal human keratinocytes (hKc) were cultivated in keratinocyte serum-free media (SFM) medium (Gibco, Invitrogen, Paisley, UK) supplemented with bovine pituitary extract (BPE), epidermal growth factor (EGF) according to manufacturer's protocol, and 100 U/mL penicillin/100 μg/mL streptomycin. All cell lines were maintained at 37°C and 5% CO_2 in a humidified incubator.

Transient transfections of HEK293AD cells were performed using jetPEI reagent (Polyplus-transfection, Strasbourg, France), whereas transient transfections of RDEB patient keratinocytes were performed using Xfect transfection reagent (Takara Bio Europe, Saint-Germain-en-Laye, France) according to the manufacturer's protocol. HEK293AD cells were cultivated in 60-mm plates and transfected with the respective Cas9/sgRNA-expressing plasmids (5 μg). Human RDEB keratinocytes were transfected with the respective Cas9/sgRNA-expressing plasmids and the minicircle DP (MC-DP) donor template in a ratio of 1:1 (1.2 μg DP and 1.2 μg sgRNA) or in case

of double-nicking in a ratio of 1:1:1 (1.2 μg DP and 1.2 μg of each sgRNA). Antibiotic selection of transfected RDEB keratinocytes was applied when cells reached 60%–80% confluency by supplementing the medium with 5 μg/mL blasticidin (Invivogene, San Diego, CA, USA). Untransfected RDEB keratinocyte cells were used as a negative control.

T7 Endonuclease I (T7EI) Assay

Mismatches upon Cas9/sgRNA-mediated DSB induction and subsequent NHEJ at the desired genomic locus in HEK293AD cells were evaluated via T7EI assays[23] (New England Biolabs, Frankfurt, Germany) on genomic DNA. Using a *COL7A1* exon 2-specific forward primer and a *COL7A1* exon 5-specific reverse primer, a 1,386-bp fragment of the *COL7A1* target locus was PCR-amplified. Digest of the resulting PCR fragment was performed according to the manufacturer's protocol (see Table S2 for primer sequences).

Flow Cytometric Analysis and Fluorescence-Activated Cell Sorting (FACS)

Transfection efficiency was evaluated 24 h–48 h post-transfection and 14 days post-selection by flow cytometric analysis using a Beckman Coulter FC500 FACS analyzer (Beckman Coulter, Brea, CA, USA). GFP (expressed from Cas9/sgRNA vector and DP vector)-expressing cells were analyzed using the Kaluza flow cytometry analysis software (Beckman Coulter).

Protein Isolation and Western Blot Analysis

2.5×10^5 RDEB keratinocytes were cultivated in keratinocyte SFM medium (Gibco, Invitrogen, Paisley, UK). Whole-cell lysates were generated by lysing the cell pellet in radioimmunoprecipitation assay buffer (RIPA buffer) (Santa Cruz Biotechnology, Heidelberg, Germany). Whole-cell lysates were centrifuged at full speed at 4°C for 20 min, and supernatant was frozen at −20°C until usage. For analysis of secreted C7, keratinocytes were grown to confluence and proteins were precipitated from cell culture supernatants as described previously.[46]

Protein samples were denatured for 5 min at 95°C in 4× loading buffer (0.25 M Tris-HCl; 8% SDS; 30% glycerol; 0.02% bromphenol blue; 0.3 M β-mercaptoethanol [pH 6.8]). Western blotting was performed as previously described.[45,47] Ponceau red (Sigma-Aldrich, St. Louis, MO, USA) staining of the nitrocellulose membrane was performed after electroblotting. Nitrocellulose membrane was blocked with blocking reagent (Roche Diagnostics, Mannheim, Germany) diluted 1:10 in Tris-buffered saline with 0.2% Tween (TBS-T) for 1 h at room temperature (RT). For detection of Cas9 protein, a monoclonal antibody raised against the N terminus of the Cas9 nuclease (C15200229) (Diagenode, Seraing, Belgium) diluted 1:1,000 in TBS-T and blocking reagent was used and incubated at 4°C overnight. For detection of C7, a rabbit anti-type VII collagen antibody (kindly provided by Dr. Alexander Nyström, Freiburg, Germany) was used at a dilution of 1:1,000. A polyclonal β-tubulin antibody (ab6064) (Abcam, Cambridge, UK) served as loading control, diluted 1:500 in TBS-T and blocking reagent. As secondary antibodies, either the horseradish peroxidase (HRP) Envision+ labeled anti-mouse or anti-rabbit antibody (Dako, Santa Clara, CA, USA) diluted 1:300 in TBS-T were used. Nitrocellulose membrane was incubated for 1 h at RT. Protein bands were visualized using the Immobilon western chemiluminescent HRP substrate (Merck, Darmstadt, Germany) and the ChemiDoc XRS imager (Bio-Rad, Hercules, CA, USA).

Immunofluorescence Staining of Type VII Collagen

1×10^5 RDEB keratinocytes were seeded into μ-Slide 8-well chamber slides (Ibidi, Gräfelfing, Germany) and grown to 70%–100% confluency. Cells were fixed with 4% formaldehyde solution (SAV Liquid Production, Flintsbach am Inn, Germany) for 10 min at RT. Permeabilization and staining of cells was performed in a single step. A rabbit anti-type VII collagen antibody (kindly provided by Dr. Alexander Nyström, Freiburg, Germany) was used in a 1:1,000 dilution, diluted in 0.3% Triton-X, blocking reagent (1:10), and TBS-T. The primary antibody was applied for 3 h at RT. After two cycles of TBS-T wash, cells were stained with an Alexa Fluor 594 goat anti-rabbit immunoglobulin G (IgG) heavy and light chain (H+L) secondary antibody (Invitrogen, Paisley, UK) (1:300 in TBS-T) for 1 h at RT. Cell nuclei were stained with DAPI (1:4,000 in TBS-T) for 10 min at RT. Finally, cells were analyzed for C7 expression, using an inverted microscope system, which includes the laser scanning confocal microscope Zeiss LSM 700 and the Axio Observer. Z1 (Carl Zeiss, Oberkochen, Germany). For cell counting and quantification of C7-positive cells, a tile scan (3 × 3 areas merged) of approximately 1,000 μm × 1,000 μm was performed.

HR Efficiency Analysis by Sub-cloning and Sanger Sequencing

For estimation of HR efficiency, we PCR-amplified the *COL7A1* target region using a forward primer binding to endogenous *COL7A1* intron 1 and a reverse primer binding to exon 5 of the *COL7A1* gene, resulting in a PCR product of 1,912 bp, which was subsequently digested with fast digest (FD) EcoRI restriction enzyme (Thermo Scientific, Vienna, Austria). To minimize the size of the PCR product and facilitate sub-cloning, a nested PCR using a forward primer binding to intron 2 and a reverse primer binding to exon 5 was performed, resulting in a PCR product of 576 bp. For sub-cloning of the PCR product, the StrataClone PCR cloning kit (Aligent Technologies, Santa Clara, CA, USA) was used according to the manufacturer's protocol. Single clones were analyzed by Sanger sequencing. ≥ 98 clones were analyzed for kinetic studies. ≥ 47 clones were analyzed for quantification of editing outcomes in RDEB keratinocytes. For detection of distinct on-target HR events, we PCR-amplified the *COL7A1* target region using three different primer sets. For all three PCRs, a forward primer binding to endogenous *COL7A1* intron 1 was used to exclude amplification of persisting DP (see Table S2 for primer sequences).

Off-Target Prediction

Off-target prediction was performed using the CRISPR RGEN Tool (Cas-OFFinder) (http://www.rgenome.net/cas-offinder/).[30] Both sgRNAs targeting intron 3 of *COL7A1* were aligned to the human target genome (GRCh38/hg38) to identify potential off-target loci (Table 1).

Next-Generation Sequencing (NGS): On-Target Region

For estimation of HR efficiency, we PCR-amplified the *COL7A1* on-target region using a forward primer binding to endogenous *COL7A1* intron 1 and a reverse primer binding to exon 5 of the *COL7A1* gene, resulting in a PCR product of 1,912 bp. To minimize the size of the PCR product for NGS analysis and to exclude amplification of the DP, a nested PCR using a forward primer binding to exon 3 and a reverse primer binding to exon 4 was performed, resulting in a PCR product of about 300 bp. NGS was performed on the Ion Torrent personal platform using the personal genome machine (PGM). Analysis of genome-editing outcomes from deep-sequencing data was implemented on the integrative genome viewer (IGV). We attained a mean coverage of about 5,000 reads per sample for the RDEB het. cell line.

Off-Target Analysis

We designed single amplicons for each off-target region (Table S2) to perform NGS analysis on the Ion Torrent PGM. A setup of 26 PCR fragments with approximately 300 bp was chosen to cover the cutting sites of the sgRNA constructs within the predicted off-target regions; predicted off-targets are listed in Table 1. The library preparation, template preparation, and the sequencing run were performed according to manufacturer's protocols (Thermo Fisher Scientific/Life Technologies, Carlsbad, CA, USA). Analysis of genome-editing outcomes from deep-sequencing data was either performed via the CRISPResso2 online platform[48] or on the IGV. We attained a mean coverage of about 5,400 reads per amplicon for the RDEB het. cell line with our off-target panel.

SUPPLEMENTAL INFORMATION

Supplemental Information can be found online at https://doi.org/10.1016/j.omtn.2019.09.011.

AUTHOR CONTRIBUTIONS

Conceptualization, T.K., U.K.; Methodology, T.K., R.N.W., U.K.; Investigation, T.K., R.N.W.; Validation, A.K.; Writing – Original Draft, T.K., R.N.W., U.K.; Writing – Review & Editing, J.R., J.W.B.; Resources, S.H., C.G.-G., A.K.; Supervision, U.K.

CONFLICTS OF INTEREST

The authors declare no competing interests.

ACKNOWLEDGMENTS

The authors thank Univ.-Prof. Dr. Eva Rohde and Karin Roider, MSc, of the Spinal Cord Injury and Tissue Regeneration Center Salzburg (SCI-TReCS) for providing their Core Facility for Microscopy. Special thanks to Dr. Alexander Nyström from the Department of Dermatology, University Medical Center, Freiburg, Germany, who kindly provided the type VII collagen antibody. We thank Bernadette Liemberger and Johannes Bischof for critically reading the manuscript. Additionally, we would like to thank Niklas Jeschko for supporting off-target sample preparation. This work was supported by DEBRA Austria.

REFERENCES

1. Fine, J.D., Bruckner-Tuderman, L., Eady, R.A., Bauer, E.A., Bauer, J.W., Has, C., Heagerty, A., Hintner, H., Hovnanian, A., Jonkman, M.F., et al. (2014). Inherited epidermolysis bullosa: updated recommendations on diagnosis and classification. J. Am. Acad. Dermatol. *70*, 1103–1126.

2. Montaudié, H., Chiaverini, C., Sbidian, E., Charlesworth, A., and Lacour, J.P. (2016). Inherited epidermolysis bullosa and squamous cell carcinoma: a systematic review of 117 cases. Orphanet J. Rare Dis. *11*, 117.

3. Petrof, G., Martinez-Queipo, M., Mellerio, J.E., Kemp, P., and McGrath, J.A. (2013). Fibroblast cell therapy enhances initial healing in recessive dystrophic epidermolysis bullosa wounds: results of a randomized, vehicle-controlled trial. Br. J. Dermatol. *169*, 1025–1033.

4. Siprashvili, Z., Nguyen, N.T., Gorell, E.S., Loutit, K., Khuu, P., Furukawa, L.K., Lorenz, H.P., Leung, T.H., Keene, D.R., Rieger, K.E., et al. (2016). Safety and Wound Outcomes Following Genetically Corrected Autologous Epidermal Grafts in Patients With Recessive Dystrophic Epidermolysis Bullosa. JAMA *316*, 1808–1817.

5. Venugopal, S.S., Yan, W., Frew, J.W., Cohn, H.I., Rhodes, L.M., Tran, K., Melbourne, W., Nelson, J.A., Sturm, M., Fogarty, J., et al. (2013). A phase II randomized vehicle-controlled trial of intradermal allogeneic fibroblasts for recessive dystrophic epidermolysis bullosa. J. Am. Acad. Dermatol. *69*, 898–908.e897.

6. Woodley, D.T., Cogan, J., Hou, Y., Lyu, C., Marinkovich, M.P., Keene, D., and Chen, M. (2017). Gentamicin induces functional type VII collagen in recessive dystrophic epidermolysis bullosa patients. J. Clin. Invest. *127*, 3028–3038.

7. Titeux, M., Pendaries, V., Zanta-Boussif, M.A., Décha, A., Pironon, N., Tonasso, L., Mejia, J.E., Brice, A., Danos, O., and Hovnanian, A. (2010). SIN retroviral vectors expressing COL7A1 under human promoters for ex vivo gene therapy of recessive dystrophic epidermolysis bullosa. Mol. Ther. *18*, 1509–1518.

8. Cong, L., Ran, F.A., Cox, D., Lin, S., Barretto, R., Habib, N., Hsu, P.D., Wu, X., Jiang, W., Marraffini, L.A., and Zhang, F. (2013). Multiplex genome engineering using CRISPR/Cas systems. Science *339*, 819–823.

9. Mali, P., Yang, L., Esvelt, K.M., Aach, J., Guell, M., DiCarlo, J.E., Norville, J.E., and Church, G.M. (2013). RNA-guided human genome engineering via Cas9. Science *339*, 823–826.

10. Zetsche, B., Gootenberg, J.S., Abudayyeh, O.O., Slaymaker, I.M., Makarova, K.S., Essletzbichler, P., Volz, S.E., Joung, J., van der Oost, J., Regev, A., et al. (2015). Cpf1 is a single RNA-guided endonuclease of a class 2 CRISPR-Cas system. Cell *163*, 759–771.

11. Gilbert, L.A., Larson, M.H., Morsut, L., Liu, Z., Brar, G.A., Torres, S.E., Stern-Ginossar, N., Brandman, O., Whitehead, E.H., Doudna, J.A., et al. (2013). CRISPR-mediated modular RNA-guided regulation of transcription in eukaryotes. Cell *154*, 442–451.

12. Vakulskas, C.A., Dever, D.P., Rettig, G.R., Turk, R., Jacobi, A.M., Collingwood, M.A., Bode, N.M., McNeill, M.S., Yan, S., Camarena, J., et al. (2018). A high-fidelity Cas9 mutant delivered as a ribonucleoprotein complex enables efficient gene editing in human hematopoietic stem and progenitor cells. Nat. Med. *24*, 1216–1224.

13. Ran, F.A., Hsu, P.D., Wright, J., Agarwala, V., Scott, D.A., and Zhang, F. (2013). Genome engineering using the CRISPR-Cas9 system. Nat. Protoc. *8*, 2281–2308.

14. Akcakaya, P., Bobbin, M.L., Guo, J.A., Malagon-Lopez, J., Clement, K., Garcia, S.P., Fellows, M.D., Porritt, M.J., Firth, M.A., Carreras, A., et al. (2018). In vivo CRISPR editing with no detectable genome-wide off-target mutations. Nature *561*, 416–419.

15. Webber, B.R., Osborn, M.J., McElroy, A.N., Twaroski, K., Lonetree, C.L., DeFeo, A.P., Xia, L., Eide, C., Lees, C.J., McElmurry, R.T., et al. (2016). CRISPR/Cas9-based genetic correction for recessive dystrophic epidermolysis bullosa. NPJ Regen. Med. *1*, 16014.

16. Hainzl, S., Peking, P., Kocher, T., Murauer, E.M., Larcher, F., Del Rio, M., Duarte, B., Steiner, M., Klausegger, A., Bauer, J.W., et al. (2017). COL7A1 Editing via CRISPR/Cas9 in Recessive Dystrophic Epidermolysis Bullosa. Mol. Ther. *25*, 2573–2584.

17. Izmiryan, A., Ganier, C., Bovolenta, M., Schmitt, A., Mavilio, F., and Hovnanian, A. (2018). Ex Vivo COL7A1 Correction for Recessive Dystrophic Epidermolysis Bullosa Using CRISPR/Cas9 and Homology-Directed Repair. Mol. Ther. Nucleic Acids *12*, 554–567.

18. Mencía, Á., Chamorro, C., Bonafont, J., Duarte, B., Holguin, A., Illera, N., Llames, S.G., Escámez, M.J., Hausser, I., Del Río, M., et al. (2018). Deletion of a Pathogenic

Mutation-Containing Exon of COL7A1 Allows Clonal Gene Editing Correction of RDEB Patient Epidermal Stem Cells. Mol. Ther. Nucleic Acids *11*, 68–78.

19. Bonafont, J., Mencía, Á., García, M., Torres, R., Rodríguez, S., Carretero, M., Chacón-Solano, E., Modamio-Høybjør, S., Marinas, L., León, C., et al. (2019). Clinically Relevant Correction of Recessive Dystrophic Epidermolysis Bullosa by Dual sgRNA CRISPR/Cas9-Mediated Gene Editing. Mol. Ther. *27*, 986–998.
20. Takashima, S., Shinkuma, S., Fujita, Y., Nomura, T., Ujiie, H., Natsuga, K., Iwata, H., Nakamura, H., Vorobyev, A., Abe, R., and Shimizu, H. (2019). Efficient gene reframing therapy for recessive dystrophic epidermolysis bullosa using CRISPR/Cas9. J. Invest. Dermatol. *139*, 1711–1721.e4.
21. Mali, P., Aach, J., Stranges, P.B., Esvelt, K.M., Moosburner, M., Kosuri, S., Yang, L., and Church, G.M. (2013). CAS9 transcriptional activators for target specificity screening and paired nickases for cooperative genome engineering. Nat. Biotechnol. *31*, 833–838.
22. Ran, F.A., Hsu, P.D., Lin, C.Y., Gootenberg, J.S., Konermann, S., Trevino, A.E., Scott, D.A., Inoue, A., Matoba, S., Zhang, Y., and Zhang, F. (2013). Double nicking by RNA-guided CRISPR Cas9 for enhanced genome editing specificity. Cell *154*, 1380–1389.
23. Kocher, T., Peking, P., Klausegger, A., Murauer, E.M., Hofbauer, J.P., Wally, V., Lettner, T., Hainzl, S., Ablinger, M., Bauer, J.W., et al. (2017). Cut and Paste: Efficient Homology-Directed Repair of a Dominant Negative KRT14 Mutation via CRISPR/Cas9 Nickases. Mol. Ther. *25*, 2585–2598.
24. Gardella, R., Belletti, L., Zoppi, N., Marini, D., Barlati, S., and Colombi, M. (1996). Identification of two splicing mutations in the collagen type VII gene (COL7A1) of a patient affected by the localisata variant of recessive dystrophic epidermolysis bullosa. Am. J. Hum. Genet. *59*, 292–300.
25. Montague, T.G., Cruz, J.M., Gagnon, J.A., Church, G.M., and Valen, E. (2014). CHOPCHOP: a CRISPR/Cas9 and TALEN web tool for genome editing. Nucleic Acids Res. *42*, W401–W407.
26. Labun, K., Montague, T.G., Gagnon, J.A., Thyme, S.B., and Valen, E. (2016). CHOPCHOP v2: a web tool for the next generation of CRISPR genome engineering. Nucleic Acids Res. *44* (W1), W272–W276.
27. Lin, Y., Cradick, T.J., Brown, M.T., Deshmukh, H., Ranjan, P., Sarode, N., Wile, B.M., Vertino, P.M., Stewart, F.J., and Bao, G. (2014). CRISPR/Cas9 systems have off-target activity with insertions or deletions between target DNA and guide RNA sequences. Nucleic Acids Res. *42*, 7473–7485.
28. Anglani, F., Picci, L., Camporese, C., and Zacchello, F. (1990). Heteroduplex formation in polymerase chain reaction. Am. J. Hum. Genet. *47*, 169–170.
29. Chen, X., Janssen, J.M., Liu, J., Maggio, I., 't Jong, A.E.J., Mikkers, H.M.M., and Gonçalves, M.A.F.V. (2017). In trans paired nicking triggers seamless genome editing without double-stranded DNA cutting. Nat. Commun. *8*, 657.
30. Bae, S., Park, J., and Kim, J.S. (2014). Cas-OFFinder: a fast and versatile algorithm that searches for potential off-target sites of Cas9 RNA-guided endonucleases. Bioinformatics *30*, 1473–1475.
31. Peking, P., Koller, U., and Murauer, E.M. (2018). Functional therapies for cutaneous wound repair in epidermolysis bullosa. Adv. Drug Deliv. Rev. *129*, 330–343.
32. Mavilio, F., Pellegrini, G., Ferrari, S., Di Nunzio, F., Di Iorio, E., Recchia, A., Maruggi, G., Ferrari, G., Provasi, E., Bonini, C., et al. (2006). Correction of junctional epidermolysis bullosa by transplantation of genetically modified epidermal stem cells. Nat. Med. *12*, 1397–1402.
33. Bauer, J.W., Koller, J., Murauer, E.M., De Rosa, L., Enzo, E., Carulli, S., Bondanza, S., Recchia, A., Muss, W., Diem, A., et al. (2017). Closure of a Large Chronic Wound through Transplantation of Gene-Corrected Epidermal Stem Cells. J. Invest. Dermatol. *137*, 778–781.
34. Hirsch, T., Rothoeft, T., Teig, N., Bauer, J.W., Pellegrini, G., De Rosa, L., Scaglione, D., Reichelt, J., Klausegger, A., Kneisz, D., et al. (2017). Regeneration of the entire human epidermis using transgenic stem cells. Nature *551*, 327–332.
35. Chamorro, C., Mencía, A., Almarza, D., Duarte, B., Büning, H., Sallach, J., Hausser, I., Del Río, M., Larcher, F., and Murillas, R. (2016). Gene Editing for the Efficient Correction of a Recurrent COL7A1 Mutation in Recessive Dystrophic Epidermolysis Bullosa Keratinocytes. Mol. Ther. Nucleic Acids *5*, e307.
36. Shinkuma, S., Guo, Z., and Christiano, A.M. (2016). Site-specific genome editing for correction of induced pluripotent stem cells derived from dominant dystrophic epidermolysis bullosa. Proc. Natl. Acad. Sci. USA *113*, 5676–5681.
37. Allen, F., Crepaldi, L., Alsinet, C., Strong, A.J., Kleshchevnikov, V., De Angeli, P., Páleníková, P., Khodak, A., Kiselev, V., Kosicki, M., et al. (2018). Predicting the mutations generated by repair of Cas9-induced double-strand breaks. Nat Biotechnol. *37*, 64–72.
38. Chakrabarti, A.M., Henser-Brownhill, T., Monserrat, J., Poetsch, A.R., Luscombe, N.M., and Scaffidi, P. (2019). Target-Specific Precision of CRISPR-Mediated Genome Editing. Mol. Cell *73*, 699–713.e6.
39. Shen, M.W., Arbab, M., Hsu, J.Y., Worstell, D., Culbertson, S.J., Krabbe, O., Cassa, C.A., Liu, D.R., Gifford, D.K., and Sherwood, R.I. (2018). Predictable and precise template-free CRISPR editing of pathogenic variants. Nature *563*, 646–651.
40. Kern, J.S., Loeckermann, S., Fritsch, A., Hausser, I., Roth, W., Magin, T.M., Mack, C., Müller, M.L., Paul, O., Ruther, P., and Bruckner-Tuderman, L. (2009). Mechanisms of fibroblast cell therapy for dystrophic epidermolysis bullosa: high stability of collagen VII favors long-term skin integrity. Mol. Ther. *17*, 1605–1615.
41. Schwieger-Briel, A., Weibel, L., Chmel, N., Leppert, J., Kernland-Lang, K., Grüninger, G., and Has, C. (2015). A COL7A1 variant leading to in-frame skipping of exon 15 attenuates disease severity in recessive dystrophic epidermolysis bullosa. Br. J. Dermatol. *173*, 1308–1311.
42. Wu, W., Lu, Z., Li, F., Wang, W., Qian, N., Duan, J., Zhang, Y., Wang, F., and Chen, T. (2017). Efficient in vivo gene editing using ribonucleoproteins in skin stem cells of recessive dystrophic epidermolysis bullosa mouse model. Proc. Natl. Acad. Sci. USA *114*, 1660–1665.
43. Liang, X., Potter, J., Kumar, S., Zou, Y., Quintanilla, R., Sridharan, M., Carte, J., Chen, W., Roark, N., Ranganathan, S., et al. (2015). Rapid and highly efficient mammalian cell engineering via Cas9 protein transfection. J. Biotechnol. *208*, 44–53.
44. Liang, X., Potter, J., Kumar, S., Ravinder, N., and Chesnut, J.D. (2017). Enhanced CRISPR/Cas9-mediated precise genome editing by improved design and delivery of gRNA, Cas9 nuclease, and donor DNA. J. Biotechnol. *241*, 136–146.
45. Peking, P., Koller, U., Hainzl, S., Kitzmueller, S., Kocher, T., Mayr, E., Nyström, A., Lener, T., Reichelt, J., Bauer, J.W., and Murauer, E.M. (2016). A Gene Gun-mediated Nonviral RNA trans-splicing Strategy for Col7a1 Repair. Mol. Ther. Nucleic Acids *5*, e287.
46. Peking, P., Koller, U., Duarte, B., Murillas, R., Wolf, S., Maetzig, T., Rothe, M., Kocher, T., García, M., Brachtl, G., et al. (2017). An RNA-targeted therapy for dystrophic epidermolysis bullosa. Nucleic Acids Res. *45*, 10259–10269.
47. Tockner, B., Kocher, T., Hainzl, S., Reichelt, J., Bauer, J.W., Koller, U., and Murauer, E.M. (2016). Construction and validation of an RNA trans-splicing molecule suitable to repair a large number of COL7A1 mutations. Gene Ther. *23*, 775–784.
48. Clement, K., Rees, H., Canver, M.C., Gehrke, J.M., Farouni, R., Hsu, J.Y., Cole, M.A., Liu, D.R., Joung, J.K., Bauer, D.E., and Pinello, L. (2019). CRISPResso2 provides accurate and rapid genome editing sequence analysis. Nat. Biotechnol. *37*, 224–226.